JGR Atmospheres

RESEARCH ARTICLE
10.1029/2021JD035485

Key Points:

- Measurement networks can quantify regional representation error and reduce uncertainty in aerosol microphysics
- Representation error varies between sites, decreases over longer averaging periods, and is higher for larger accumulation mode aerosols
- Local meteorology introduces heterogeneity in aerosol surface area and size distributions across a rural, continental background region

Supporting Information:

Supporting Information may be found in the online version of this article.

Correspondence to:

E. Asher,
elizabeth.asher@noaa.gov

Citation:

Asher, E., Thornberry, T., Fahey, D. W., McComiskey, A., Carslaw, K., et al. (2022). A novel network-based approach to determining measurement representation error for model evaluation of aerosol microphysical properties. *Journal of Geophysical Research: Atmospheres*, *127*, e2021JD035485. https://doi.org/10.1029/2021JD035485

Received 8 JUL 2021
Accepted 2 NOV 2021

Author Contributions:

Conceptualization: Troy Thornberry, David W. Fahey, Allison McComiskey, Kenneth Carslaw, Ru-Shan Gao
Data curation: Elizabeth Asher
Formal analysis: Elizabeth Asher, Sophie Grunau, Kai-Lan Chang, Hagen Telg
Investigation: Elizabeth Asher
Methodology: Elizabeth Asher, Troy Thornberry, Ru-Shan Gao
Project Administration: Troy Thornberry, David W. Fahey, Allison McComiskey, Ru-Shan Gao
Resources: Troy Thornberry, Allison McComiskey, Ru-Shan Gao

© 2021. American Geophysical Union. All Rights Reserved. This article has been contributed to by U.S. Government employees and their work is in the public domain in the USA.

A Novel Network-Based Approach to Determining Measurement Representation Error for Model Evaluation of Aerosol Microphysical Properties

Elizabeth Asher[1,2], Troy Thornberry[2], David W. Fahey[2], Allison McComiskey[3], Kenneth Carslaw[4], Sophie Grunau[4], Kai-Lan Chang[2], Hagen Telg[5], Ping Chen[6], and Ru-Shan Gao[2]

[1]Cooperative Institute for Research in Environmental Sciences at the University of Colorado Boulder, Boulder, CO, USA, [2]NOAA Chemical Sciences Laboratory, Boulder, CO, USA, [3]Brookhaven National Laboratory, Upton, NY, USA, [4]University of Leeds, Leeds, UK, [5]Cooperative Institute for Research in Environmental Sciences, Global Monitoring Laboratory, Boulder, CO, USA, [6]Handix Scientific, Boulder, CO, USA

Abstract Atmospheric aerosol size and abundance influence radiative effects and climate change. To date, efforts to constrain global climate models' radiative forcing with in situ aerosol observations have been hamstrung by uncertainty. One source of error, the regional "representation error," arises when accurate but sparse single-point measurements of atmospheric aerosol distributions are compared with a model value, assuming that the single-point measurement is representative of the model domain. The Portable Optical Particle Spectrometer network in the Southern Great Plains (POPSnet-SGP) campaign has demonstrated that a network of nearly autonomous aerosol instruments operating at ambient temperature and relative humidity (with low measurement error) may be used to quantify measurement representation error and investigate the factors introducing heterogeneity in aerosol distributions across a rural, continental background region. Measurements were made using Portable Optical Particle Spectrometer (POPS) instruments at several sites for five months across the Department of Energy's Aerosol Radiation Measurement Southern Great Plains (ARM-SGP) User Facility in the central USA. Measurement representation error decreased with longer averaging periods (20%–40% between 1 s and 1 day), varied between sites by 10%–20% for aerosol concentration 140–2,500 nm in diameter (N_140), and was higher for aerosols >400 nm in diameter (N_400). Our measurements also show the influence of local meteorology on aerosol surface area (A_140) and size distributions: A_140 is positively correlated with wind speed and relative humidity, negatively correlated with precipitation, and lower given westerly winds. We conclude that the POPSnet approach provides considerably more insight into the spatial variability in the aerosol population that can be used to constrain climate models than would be available from similar networks of PM 2.5 monitors.

Plain Language Summary Global climate models have long struggled to predict the radiative effects of aerosols on climate. In addition to measurement error and model error, model-observation comparisons may suffer from error related to a sample's representativeness of the aerosol population. This study outlines an approach to quantify the representation error, using the Southern Great Plains (SGP) as a testbed, and find that to an extent, observed differences are related to local meteorology.

1. Introduction

Aerosols are heterogeneously distributed in the atmosphere, influencing weather and climate in numerous ways (Haywood & Boucher, 2000; Lohmann & Feichter, 2005). Decades of research have not effectively reduced the uncertainty in aerosol-cloud radiative effects, inhibiting major improvements in climate model predictions (Bellouin et al., 2020). Model intercomparison projects have demonstrated that models exhibit a wide range of simulated aerosol microphysical properties, as compared with simulated aerosol optical properties (Mann et al., 2014; Myhre et al., 2009) or trace gas constituents, which are fundamental to a model's ability to predict aerosol radiative effects and cloud-nucleating properties. The distribution of accumulation mode aerosol size and abundance have been identified as a key driver in aerosol radiative forcing, particularly in the boundary layer (BL) in the continental US, removed from the influences of marine sulfur emissions and volcanic emissions (Andrews et al., 2006; Carslaw et al., 2013).

Software: Elizabeth Asher
Supervision: Troy Thornberry, David W. Fahey, Ru-Shan Gao
Validation: Elizabeth Asher
Visualization: Elizabeth Asher
Writing – original draft: Elizabeth Asher
Writing – review & editing: Elizabeth Asher, Troy Thornberry, David W. Fahey, Allison McComiskey, Kenneth Carslaw, Kai-Lan Chang, Hagen Telg, Ru-Shan Gao

Simplistic model-observation agreement is not a good gauge of model accuracy (Carslaw et al., 2013). Seeking to maximize global coverage with respect to cost, networks of research-grade instruments (e.g., AERONET, IMPROVE, and others) have been sparsely distributed. Comparisons between models with low spatial resolution and in situ point measurements may lead to representation error—when a heterogeneously distributed atmospheric component is randomly sampled within a model grid cell, and this sample does not accurately represent the population mean but is compared as if it does. For instance, the sample may be instead persistently higher, as with scientific instruments sited for air quality applications in polluted locations within the model grid cell domain. This concept was first unpacked in numerical weather prediction (e.g., Lorenc, 1986) and has since been used widely to describe an important source of error in data assimilation across many fields, including atmospheric sciences (Janjić et al., 2017). With respect to aerosols, the representation error has so far been estimated by comparing high-resolution models (standing in for observations of real-world variability) with low-resolution global models with grid cell dimensions on the order of 100 km (Reddington et al., 2017; Schutgens et al., 2017). These studies estimate that the relative monthly representation error in Oklahoma is ∼25% for PM 2.5 but higher (∼40%) for aerosol number concentration (>10 μm) at the surface. The representation error has been shown to be an important limiting factor in the observational constraint of a global aerosol model in which statistical methods are used to rule out observationally implausible model behavior (Johnson et al., 2020). The representation error is likely to vary enormously around the world depending on the heterogeneity of aerosol sources and sinks, as well as local meteorology, and to date, has not been estimated using measurements.

Measurement error (or total measurement uncertainty) sets the limit on the detectability of systematic differences that would lead to representation error. Traditionally, tradeoffs have existed for model evaluation between the data richness (e.g., detailed information, for instance, on the full aerosol size distribution, vertical resolution, horizontal spatial resolution, and temporal resolution) and reliability of an instrument and its cost of deployment. Spatially dense networks of low-cost sensors, seeking to understand spatial variability in both aerosols and trace gases for better predictions of air quality, have been widely criticized for their inaccuracy, poor precision, and instrument drift (Bulot et al., 2019; Piedrahita et al., 2014). To date, the high cost associated with a deployment involving numerous research-grade aerosol instruments for aerosol microphysics has rendered this observational approach impractical.

Here, we describe the first deployment of an archetypical, spatially dense network of lower-cost, but robust, research-grade aerosol instruments—the Portable Optical Particle Spectrometer (POPS; Gao et al., 2016)—to directly assess aerosol heterogeneity over a global model grid-cell-sized domain. The pilot network, POPS-net-SGP, is deployed at the Department of Energy's Aerosol Radiation Measurement Southern Great Plains (ARM-SGP) User Facility (36.607 N, 97.488 W) which covers ∼150 km × 150 km in northern central Oklahoma. The POPS network seeks to determine the feasibility of such networks and to address two major needs in atmospheric aerosol science: (a) the need to determine whether representation error is important in model-observation comparisons in various environments, beginning with the Southern Great Plains SGP region and (b) the need for measurements of accumulation mode aerosol size and abundance to constrain aerosol radiative effects, particularly in rural, background continental air masses. Logistical considerations contributed to choosing ARM-SGP as the location for this pilot network, including its infrastructure, available ancillary measurements, and the rich history of atmospheric science in this region. For example, the bulk index of refraction, which influences aerosol sizing, has been characterized over the Southern Great Plains (Aldhaif et al., 2018; Ferrare et al., 1998), and other factors that influence Earth's radiation budget, such as the surface albedo, have been well studied (Li, 2002; Michalsky et al., 2003) and are regularly quantified.

For the purposes of comparing with global aerosol models, we define a spatially dense network as one site per 5,000 km^2, equivalent to five or more sites (the required density will vary with location) scattered within a ∼150 km × ∼150 km area (approximately the size of a global model grid cell). Our approach includes operating two POPS side-by-side whenever possible at each site to quantify measurement error. We also calculate the possible systematic error in aerosol sizing that would result from an incorrect assumption regarding the bulk index of refraction (see Supporting Information S1 for details). We examine factors that might contribute to the observed differences in aerosol distributions across a region, including local meteorology, transport, and the primary aerosol emissions.

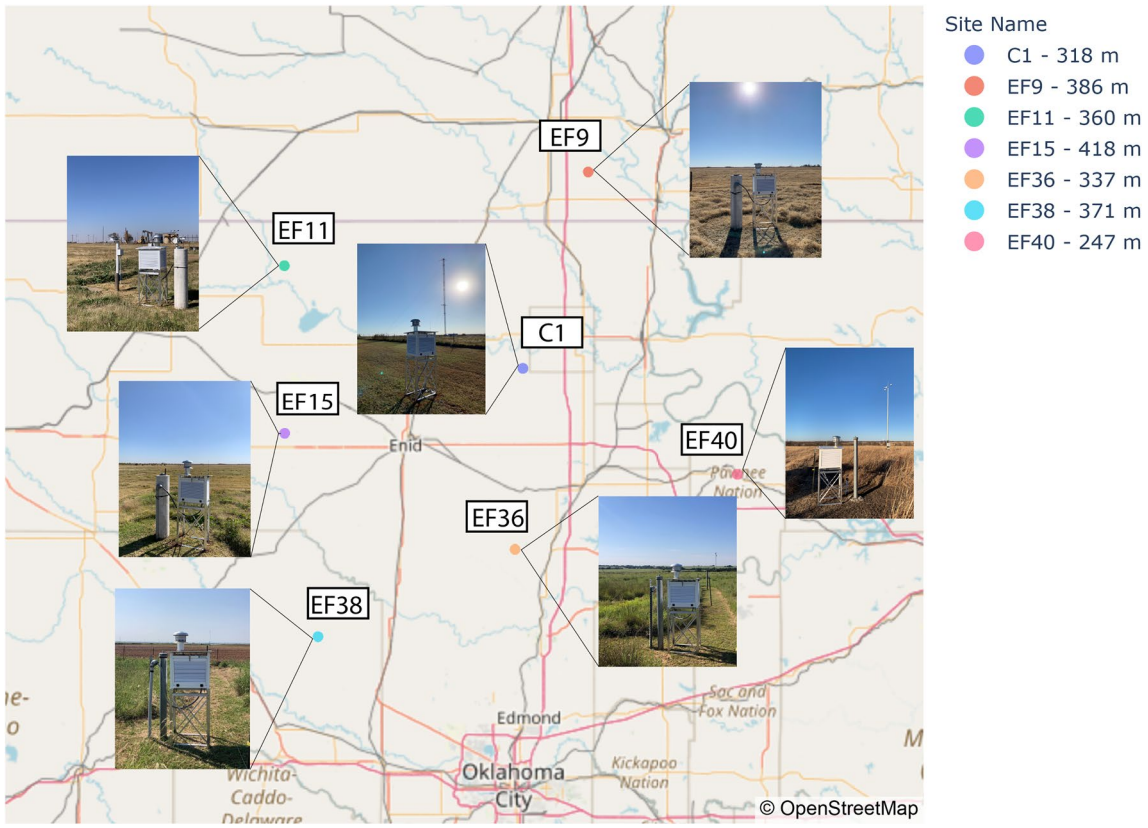

Figure 1. Locations and photos of Portable Optical Particle Spectrometer network in the Southern Great Plains (POPSnet-SGP) enclosures installed at the central facility (C1) and six extended facility (E/EF) sites (a). Sites are located in rural areas and shown in different colors, with the altitude of each listed in meters.

2. Methods

2.1. Network Description

POPSnet-SGP comprises seven sites in northern Oklahoma, including the ARM-SGP central facility and six extended facility sites (with one across the Oklahoma-Kansas border). These sites are distributed across a ~150 km × ~150 km region, spanning the latitude range 35.86–37.15 N and longitude range 96.76–98.36 W, with altitudes between 247 and 418 m above sea level (Figure 1a). The ARM-SGP region is relatively homogenous with respect to terrain and climate (Sisterson et al., 2016). Annual mean temperature ranges between 14.4 and 15.6 °C, and annual precipitation varies from ~760 to 1,020 mm yr^{-1}. Winds at ARM-SGP have a large N-S component at all POPSnet-SGP stations (Figure S1 in Supporting Information S1), and photographs from each POPSnet site depict each POPSnet enclosure surrounded by largely flat, grassy terrain, with some trees and taller vegetation (Figure 1a). Accumulation mode aerosol (0.1–2.5 μm) accounts for a considerable fraction of the total aerosol concentration observed at ARM-SGP due to cloud processing: evaporating cloud droplets leave behind particles >0.1 μm in diameter (Nobel & Hudson, 2019).

POPS is a high-sensitivity instrument that sizes individual particles within the range of 0.14–2.5 μm based on the scattered light produced as each particle passes through a focused laser beam and segregates these signals into 1 of 24 (as configured for this study) specified size bins (Table S1 in Supporting Information S1; Gao et al., 2016). The instrument flow rate is used to calculate the particle concentration (cm^{-3}) in each size bin, as well as the aerosol surface area density of each bin ($\mu m^2\ cm^{-3}$). The binned particle concentrations and surface area densities are summed to yield the aerosol number concentration (N_140) and surface area (A_140) within the POPS' size range. For details on the calculated uncertainty in N_140 and A_140, see Supporting Information S1.

Autonomous, nearly continuous operation of POPSnet-SGP was achieved from mid-October through mid-March (QA/QC'ed data only are shown here; Figure S2 in Supporting Information S1). Throughout the period considered,

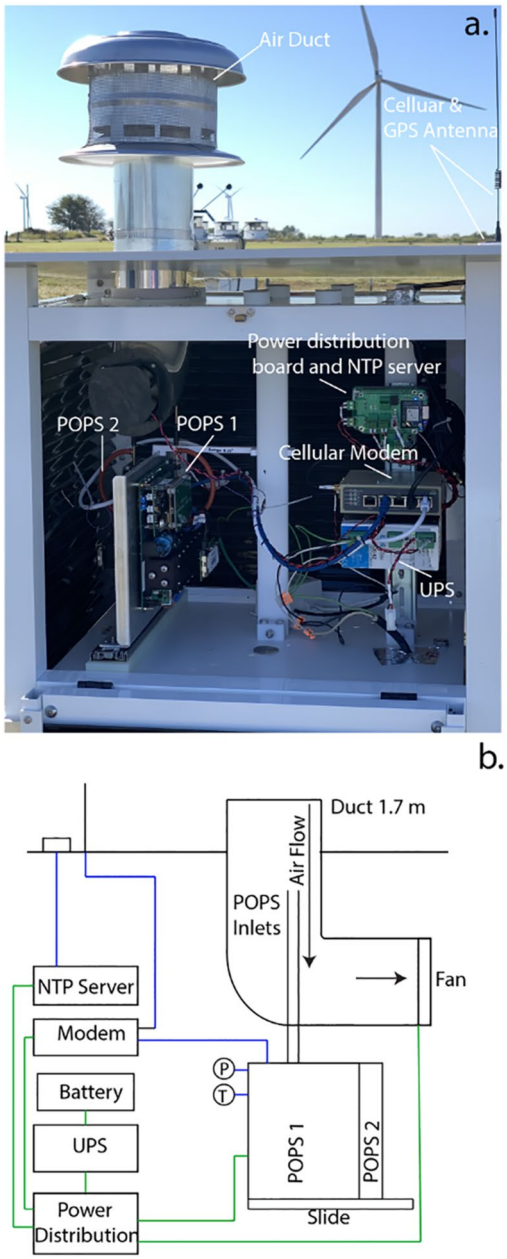

Figure 2. Labeled photo (a) and schematic (b) of a Portable Optical Particle Spectrometer network in the Southern Great Plains (POPSnet-SGP) enclosure. In the schematic, the plumbing is shown from a sideview, and electrical power connections are shown in green and data transfer is shown in blue.

five of seven sites were often operational, each of which included two POPS operating side-by-side (Figure 2). The POPSnet enclosures are Stevenson screen meteorological instrument shelters (Met 01, MetSpec Ltd, UK), selected for their surface reflectivity, durability, and good airflow, which help maintain ambient temperature (and thus RH) within them. Outside air for aerosol sampling is drawn into the enclosure through an air duct (10.45 cm ID) from a height of 1.7 m by a fan at a speed of 1–1.5 m s^{-1} (Figure 2), which is similar to the POPS instrument inlet flow speed. Within the enclosure, two POPS are mounted vertically (inlet-up) back-to-back on an aluminum plate (Figure 2). The POPS inlets are aligned vertically and subsample air from near the center of the air duct, each at a rate of ~3 cm^3 s^{-1} above the 90° bend in the air duct (Figure 2b). Uninterrupted, clean power is supplied using a UPS (Bell LBD 120-12) with a backup battery (14.8 V Tenergy) in case of power outages. The POPS instruments share a local area network (LAN) with a cellular modem (Inhandnetworks IR615). A single board computer (Beagle Bone Black Industrial) connected to a GPS receiver (Adafruit) is used as a time server to maintain synchronization of the POPS real-time clocks, connected to the two POPS through the LAN.

The cellular modem transmits near real-time processed 1-s data to the NOAA server, where it is stored, and subsequently archived. The most recent 1-s data, hourly, and daily averaged data from each POPS (updated every night at midnight) may be viewed online (https://csl.noaa.gov/projects/popsnet/data/). The NTP server, power distribution board, cellular modem, and UPS are mounted to a vertical DIN rail (Figure 2). The POPS units on the aluminum plate are mounted to a slide that can extend outside of the enclosure, facilitating the installation, and routine maintenance of POPS, as well as the retrieval and archival of raw per-particle data from a USB port on each instrument. The mounting configuration has room to accommodate additional miniaturized instruments (Figure 2).

2.2. Quantifying Measurement Representation Error

The network mean is a proxy for the true regional value and a good basis for future model evaluation. Measurement representation error ($\bar{\epsilon}_{S,t}$), which can be calculated for any averaging period (or time period, t) and station (S), is calculated as the normalized difference between station observation, $\overline{O}_{S,t}$ (e.g., A_140, N_140, N_400) and the network mean, $\overline{N}_t$ (Equation 1; adapted from Schutgens et al. (2017, Equation 5))

$$\bar{\epsilon}_{S,t} = (\overline{O}_{S,t} - \overline{N}_t)/\overline{N}_t \quad (1)$$

If we assume that a reduced time-resolution (i.e., temporally averaged) network mean data product is directly comparable to a coarse model grid point value, then we can calculate the representation error associated with using any single site rather than the network mean. Model representation error could be calculated by substituting model output for the network mean. This simple quantification provides information on the fractional error attributable to representativeness at each station and the variability between sites and over time in that error.

2.3. General Additive Model for Time Series Analysis

We use general additive models (GAM) implemented using the R package *mgcv* (Wood, 2017) to decompose the temporal elements (months, days, hours) of correlated aerosol (A_140) time series across POPSnet-SGP and test for the influence of local meteorological (and spatial) variables on the time series at each site. A GAM

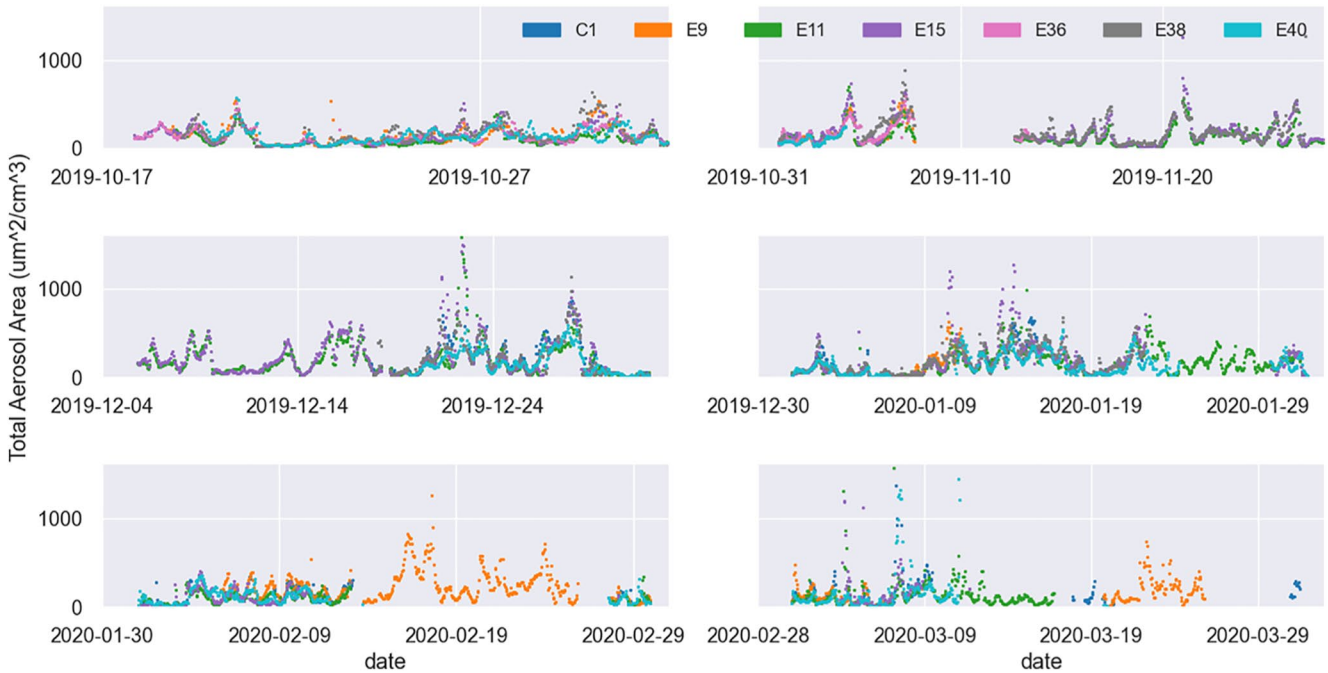

Figure 3. Hourly mean A_140 from each Portable Optical Particle Spectrometer network in the Southern Great Plains (POPSnet-SGP) site from mid-October 2019 to mid-March 2020, including all available QA/QC'ed 1-min averaged (arithmetic mean) data, with each panel showing a separate month. Data gaps are related to server failures and data quality assurance.

is an extension of the multivariate linear model where each linear predictor variable can be replaced by a functional form: it comprises an overall intercept and a linear combination of spline functions involving the predictor variables that best predict the response variable, which in this case is near surface A_140. The type of spline functions should be selected by the nature of the predictor variable; here, we use two types of spline functions, one is cubic regression splines for modeling any nonlinearity between the response and variable, another is cyclic cubic regression splines for representing any periodic pattern (e.g., capturing potential diurnal variability in near surface A_140; Equation 1). Our predictors include the consecutive day (since 15 October; D), the hour (H), longitude (Lon) and the local meteorological parameters of relative humidity (RH), temperature (T), wind speed (Ws), wind direction (Wd), and precipitation (P) (Equation 2)

$$E(Y) = \beta_0 + f_1(D) + f_2(H) + f_3(Lon) + f_4(RH) + f_5(T) + f_6(Ws) + f_7(Wd) + f_8(P) \quad (2)$$

where the response is based on 1-min data. To avoid potential overfitting resulting from a large set of predictor variables, a roughness penalty was applied to each functional approximation (so the model will not seek to capture unstructured or noisy variation in the response and the result is more generalizable; Chang et al., 2020), and the model is fitted by the generalized cross validation (GCV) criterion (Wood, 2017).

3. Results and Discussion

3.1. Temporal and Spatial Variability in Surface Aerosol Size Distributions in the Southern Great Plains

We observed spatial and temporal variability in aerosol size distributions across the SGP continental background region between October and March. Surface area is a useful metric because it is related to both aerosol heterogenous chemistry and its radiative effects. Across all sites between October and March (given a 1-hr averaging period), A_140 ranged from <5 to >1,500 $\mu m^2\ cm^{-3}$, and exhibited considerable temporal variability each month (Figure 3). These measurements indicate overall good coherence between near-surface aerosol observations across our study area, although disparities existing between hourly time series from each station (Figure 3). The network mean represents the arithmetic mean of (A_140, N_140, or N_400) time series from each site. Measurement error is calculated as the arithmetic mean of between pairs of POPS at the stations (assumptions in aerosol sizing are not pertinent for N_140; Equation 3 in Supporting Information S1; Figure S4 in Supporting Information S1).

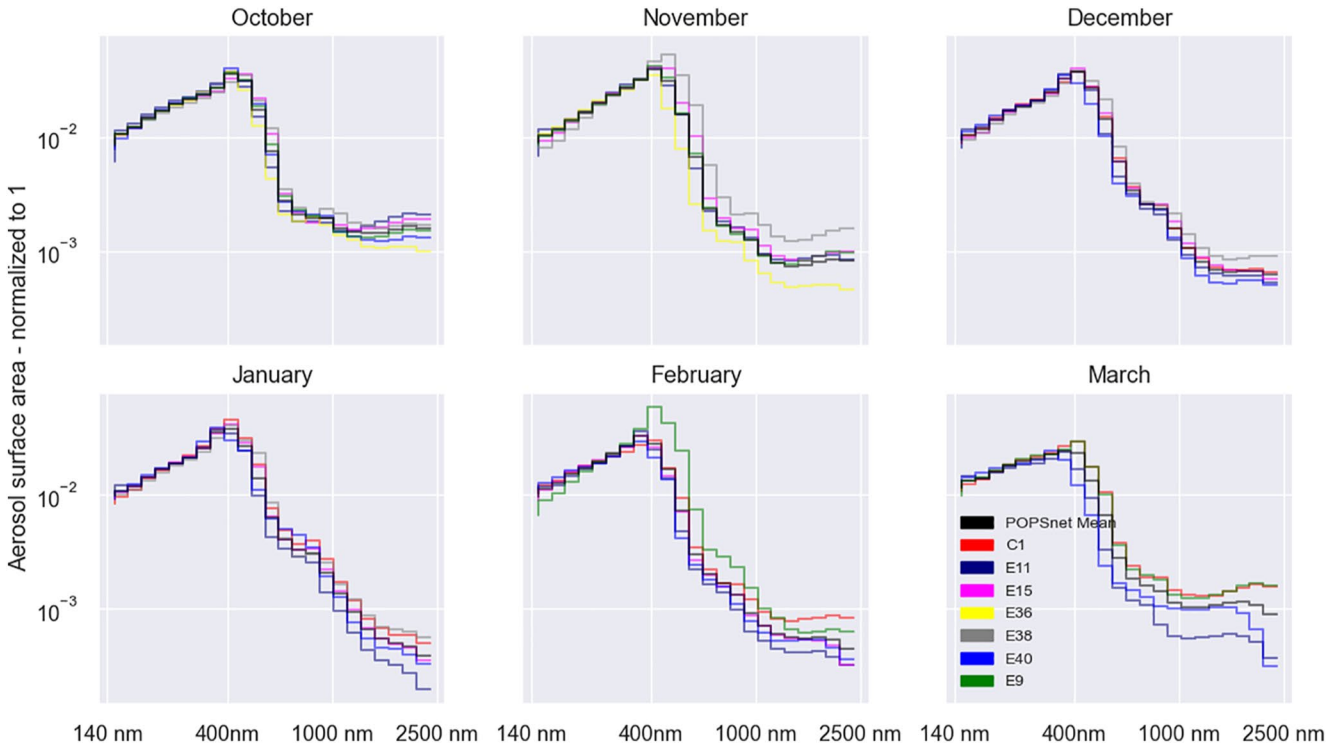

Figure 4. Monthly median normalized (to one) surface area size distributions from 1-min arithmetically averaged Portable Optical Particle Spectrometer network in the Southern Great Plains (POPSnet-SGP) data from October to March. Median distributions depicted represent periods when all stations shown were operating (no missing data). Note the log-log scale.

On average across all sites, measurement error during this period remained low for N_140 (4.5% ± 3.2%) and A_140 (7.9% ± 6.7%) (mean ± 1σ). Confidence in estimates of representation error scale with measurement error or measurement uncertainty. For example, hourly A_140 from stations E11 and C1, e.g., exceeds the network mean ± the total measurement uncertainty in A_140 ≤ 27% of the time (Figure S4 in Supporting Information S1) (the total measurement uncertainty in A_140 includes possible error related to assumption on the bulk index of refraction, see Equation S3 in Supporting Information S1 for details); however, hourly N_140 from these stations exceeds the network mean aerosol concentration ± the measurement error in N_140 78%–79% of the time.

Aerosol surface area size distributions could result in different radiative effects due to different scattering efficiencies of different size aerosols (Murphy et al., 2021), and could provide insight into aerosol sources, for instance if the distribution became significantly bimodal. From the goal of providing a measurement for model aerosol representation, the size distribution imposes more constraints on the model. Median (normalized to one) surface area size distributions for October-March (calculated using 1-min arithmetically averaged data when all stations shown were in operation) indicate that the peak in surface area size distributions in the fine/accumulation mode routinely occurred at an average particle diameter of ~390 nm and within the range of 330–410 nm between mid-October 2019 and mid-March 2020 (Table S1 in Supporting Information S1; Figure 4). At sites E15 and E38, located in western central Oklahoma (Figure 1), aerosols with diameters >400 nm contributed more to the overall surface area than the network mean (Figure 4), also leading to higher A_140 at these sites than other individual sites (Figure 3) between October and January. As discussed below, we hypothesize that low soil moisture and sandy soil in the westernmost part of the state (Parworth et al., 2015) may help explain the observed differences in size distributions.

3.2. Representation Error in the Southern Great Plains

This campaign indicates that a spatially dense network of aerosol instruments with low measurement error (e.g., 4.5% ± 3.2%; mean ±1σ for N_140) may be used to quantify measurement representation error in a continental background region. Our approach may be used moving forward to quantify the model representation error and

constrain additional sources of model error, when model output is compared with the network mean. Analysis of data collected from mid-October 2019 to mid-March 2020 generated three significant findings: the measurement representation error (a) decreases for surface aerosol concentrations across POPSnet-SGP with increasing averaging periods, (b) is higher for accumulation mode aerosols with diameter >400 nm, and (c) varies by site. These findings are expanded upon in this section.

The network average representation error at various data averaging periods (e.g., 1 s–1 day; a), the representation error at various sites (b), and the root mean squared error (RMSE) of A_140 time series (c) are summarized in Figure 5. POPSnet-SGP representation error decreased when data were averaged over longer time periods, and the largest decrease occurs between 6 hr and 1 day, with the greatest impact on the tails of the distributions (Figure 5a). The representation error is larger for N_400 (e.g., in a 30-min averaging period it is <±89% as opposed to <±69% for N_140), due primarily to differences in concentrations of medium sized accumulation mode aerosols (410–670 nm; Figure S5 in Supporting Information S1). Measurement representation error distributions were approximately normally distributed around zero; if model representation error was calculated, we might expect to see median values farther from zero, due to model bias. Our data also suggest that a single site may be more or less "representative" than others. The mean representation error at each site varies between −4% and 10% for N_140%, −10% and 13% for A_140%, and −19% and 22% for N_400 given a 30-min averaging period (Figure 5b). Representation error at each site is also systematically more variable for N400 (1σ = 28–51%), compared with N_140 (1σ = 27–37%; Figure 5b).

The RMSE of A_140 enables us to compare variability between sites, which may have values below or above the network mean, on the same scale (Figure 5c). In addition, the RMSE is not normalized, and as a result is more sensitive to outliers. Like representation error, station A_140 time series' RMSE decreased with increasing averaging periods, with the sharpest decrease occurring between 6 hr and 1 day. The RMSE also varies with site selection, also indicating that measurements at a single station may be more (e.g., C1) or less (e.g., E38) representative of the larger region than the "average" station at various averaging periods (Figure 5c). Together Figures 5b and 5c indicate that C1 is a good location for regional studies, as it is representative with respect to total aerosol concentration and surface area and has a lower RMSE than the "average" station.

Ground-based networks may still offer advantages over a single well-chosen site when comparing to observations with larger regional footprints or model output. Because horizontal wind speeds generally increase with altitude in the BL, column, tall tower, and aircraft observations represent larger spatial scales than ground-based measurements. Accordingly, such measurements may correspond better with a ground-based network mean than with ground-based measurements from a single site, even one that is more representative than most. AERONET fine mode aerosol optical depth (AOD) at the central facility is correlated with POPSnet surface A_140 (Figure S6 in Supporting Information S1). The relationship of fine mode AOD to the POPSnet mean A_140 is very similar to that to C1 A_140; however, the relationship to the POPSnet mean is statistically stronger (Figure S6 in Supporting Information S1; note the number of observations is the same). We hypothesize that differences of representativeness between the network mean and even a well selected location would grow in regions that are less homogenous with respect to landscape, meteorology, and industry. In Sections 3.3 and 3.4, we discuss how local meteorology across POPSnet-SGP plays an important role in differences of representativeness.

3.3. Influence of Local Meteorology on Aerosol

On short time scales, meteorology exerts a strong effect on aerosol size and abundance and A_140 at SGP, which is well summarized by a general additive model (GAM) using data from each station binned by 1-min increments (Equation 1; Table 1; Figure 6). The selected model includes temporal and meteorological parameters (Adj. r^2 = 0.45; GCV = 1.5E16; n = 570,447), where all individual predictors were considered significant (p < 2.0E−16). A significant portion of the variance was explained by meteorological predictors alone (Table 1).

Natural spline relationships between each predictor and the A_140 are shown (Figure 6) that together make up this GAM. Relative humidity is directly related to A_140, likely due to the hydroscopic growth and shrinkage of aerosol—this relationship appears almost linear; however, the slope of the relationship drastically increases when RH > 80%. Precipitation is inversely related to total aerosol A_140, due to aerosol scavenging in water droplets. Sites located further west in POPSnet-SGP had higher total aerosol A_140 on average, potentially due to sandier soils (Parworth et al., 2015) in the western part of our study area. On average, higher wind speed

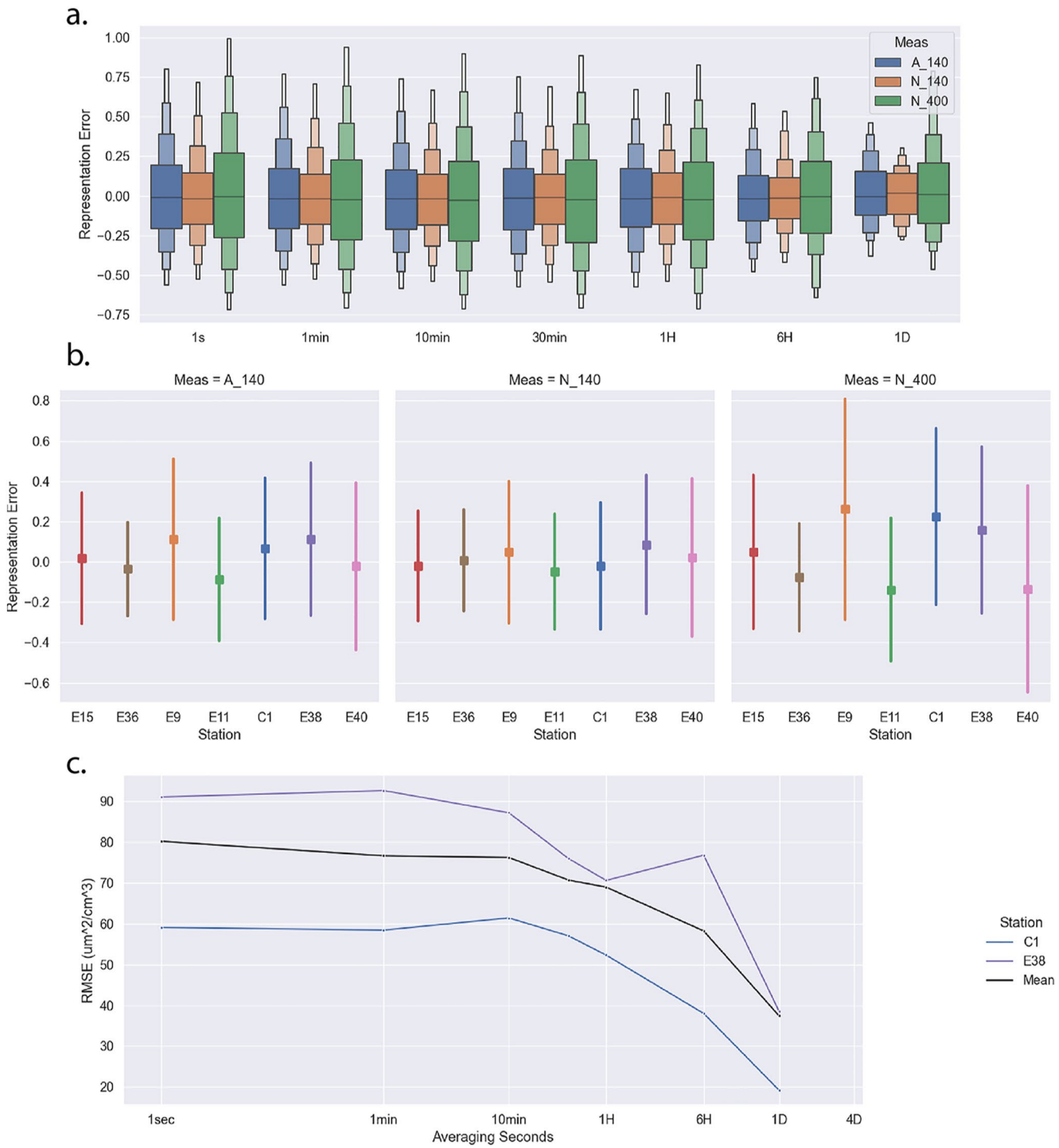

Figure 5. Letter value plots (a) showing representation error distribution across all stations (quantiles 0.05, 0.0625, 0.125, 0.25, 0.5, 0.75, 0.875, 0.935, 0.95) for total aerosol concentration, total aerosol concentration greater than 400 nm and total aerosol surface area as a function of averaging period. The mean and standard deviation of representation error for total aerosol concentration, aerosol concentration with diameter >400 nm, and aerosol surface area from each station with an averaging period of 30 min (b). The mean root mean squared error (RMSE) from two stations within the network and the mean of all stations within the network, as a function of averaging period (c). All data between mid-October and mid-March with ≥4 operational stations were used for this analysis.

Table 1
Model Selection Parameters for GAM Models

	Standard error	*T* value	*p*-Value	
Intercept	1.6E6 (1.7E6)	1,100 (1,000)	<2E−16	Adjusted R^2
1.8E9	Estimated DF	*F*-Statistic		0.45 (0.37)
S(*D*)	27 (NA)	2,300 (NA)	<2E−16	
S(*H*)	21 (NA)	54 (NA)	<2E−16	GCV
S(*D*, *H*)	26 (NA)	260 (NA)	<2E−16	1.5E16 (1.7E16)
S(*Lon*)	4.0 (4.0)	4,400 (4,800)	<2E−16	
S(*RH*)	5.9 (8.7)	33,000 (27,000)	<2E−16	Var. explained
S(*T*)	7.0 (8.0)	1,200 (1,200)		45% (37%)
S(*Ws*)	7.8 (8.5)	300 (280)	<2E−16	
S(*Wd*)	13 (13)	1,900 (2,000)	<2E−16	Observations *n*
S(*P*)	2.0 (2.0)	830 (1,000)	<2E−16	570,447

Note. The selected model used to explain 1-min data, shown in Equation 1, is compared with a GAM that includes only spatial and meteorological parameters shown in parentheses (e.g., *Lon*, *RH*, *T*, *Ws*, *Wd*, and *P*).

also leads to higher total aerosol A_140, likely because higher wind speeds may lead to higher primary aerosol emissions (e.g., from dust), and westerly winds result in lower total aerosol A_140, potentially due to increasingly rural landscape from east to west (i.e., fewer major town or cities to the west than to the north, east, or south; Figure 1a). The relationship between wind speed and wind direction and total aerosol A_140 at each station is shown in more detail in Figure S7 in Supporting Information S1; quantiles in the aerosol A_140 are positively correlated with wind speed, but the strength of this relationship (i.e., slope) differs based on the wind direction and is lowest given westly winds. Slightly higher A_140 is observed during the day, often peaking at midday. A significant portion of aerosol variance is event driven (i.e., depends on the day and time; Figures 3 and 6b and 6c), and may relate, e.g., to aerosol transport across POPSnet-SGP, as discussed in more detail in Section 3.4.

We note that some sources of variance in the A_140 are excluded from the GAM, such as differences that arise due to soil type, land use (e.g., farming or ranching) and local gravel road traffic. For instance, we cannot use the GAM to represent localized primary aerosol emission and subsequent increase in A_140 that would result from a truck driving by on an upwind gravel road. In addition, the total uncertainty (i.e., the sum of potential systematic errors that could result from incorrect assumptions of the index of refraction and measurement error, defined as the difference between paired POPS measurements) could also be part of the variance that the GAM is unable to explain.

3.4. Case Studies—A_140 and Size Distributions

The relationships identified by the GAM and its limitations are best illustrated by concrete examples selected from the POPSnet-SGP time series. Paired POPS measurements highlight the spread A_140 time series over short time periods (Figure 7), and hourly (number) size distributions over 24-hr during three of these six time periods from five sites add insight into these events (Figure 8). Discrepancies in the aerosol (number) size distributions and ancillary meteorological data from each site provide evidence as to whether these anomalies were likely driven by aerosol transport, hygroscopic growth, wet deposition, or local primary aerosol emissions.

Hydroscopic growth and scavenging of aerosol are inferred based on corresponding patterns in RH and precipitation with number concentration size distributions. For instance, on 30 October 2019 moderate northerly winds (Figure S8) transported small (∼200-nm diameter) aerosols from ∼8 am at E11 to E15 by ∼10 am, which continued to grow rapidly in size (Figures 7 and 8), potentially due to high RH (>90%; Figure S9 in Supporting Information S1). That same morning, higher number concentrations in aerosols <400 nm were observed at E9 than at E40 (E9 is located north of E40; Figure 8). The sparsity of aerosols at E40 from midnight to 8 am followed persistent and somewhat local heavy precipitation (Figure S9 in Supporting Information S1).

Offset timing of similar aerosol distributions may correspond with transport in the mean wind direction. On 22 December, during a period of westerly winds (Figure S8 in Supporting Information S1), we observed anomalously high number concentrations of fine mode aerosols <700 nm for a 1-day period (Figures 7 and 8). We observed elevated number concentrations in aerosols >700 nm at E11, E15, and several hours later (albeit, much lower total concentrations), at E40 (Figure 8).

On 5 January 2020, we observed an atypical pulse in A_140 first at E15 and then at E11 (Figure 7). At E15 between 12 and 2 a.m., and then later at E11 between 2 and 4 a.m., we recorded an increase number concentration of aerosols from 140 to 500 nm in diameter (Figure 8). Southerly winds prevailed during this period (Figure S8 in Supporting Information S1), and we hypothesize that this pulse represented a large, local primary emission near E15, which was later transported across E11 (we note that this pulse was not observed at other POPSnet-SGP sites, including E38 on the night of 4 January 2020). Later that day, we again witnessed the growth (and shrinkage) of accumulation mode aerosols, potentially related to changes in RH (Figure S9 in Supporting Information S1; no precipitation was observed at this time).

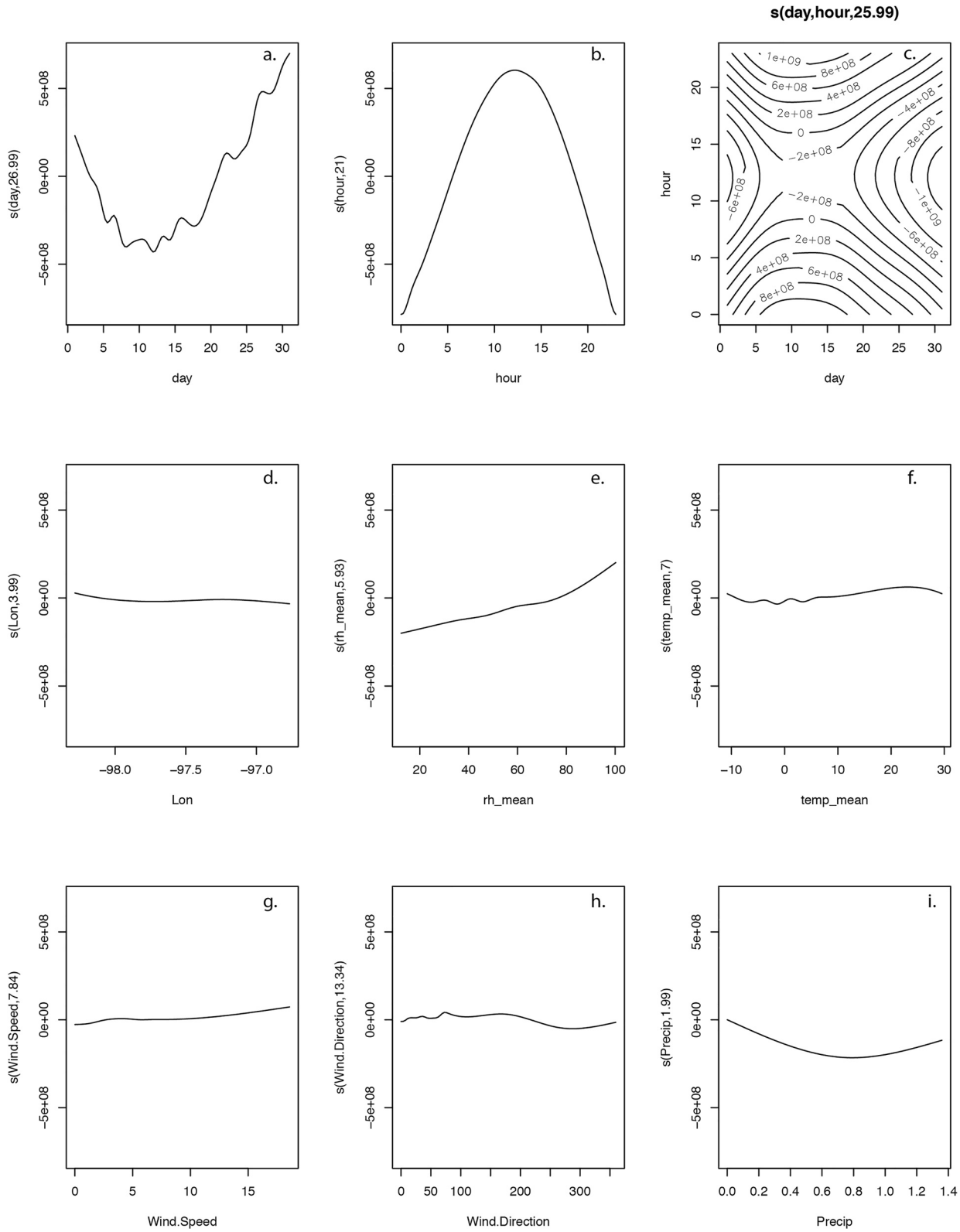

Figure 6. Flexible, smooth nonlinear component functions between aerosol A_140 (1 min) correlated time series from across Portable Optical Particle Spectrometer network in the Southern Great Plains (POPSnet-SGP) and predictor variables from the selected general additive models (GAM; Equation 1). Predictor variables include both temporal elements of the time series (i.e., consecutive days and hours) and meteorological (and spatial) variables (e.g., relative humidity (*RH*)). As is typical, the response is scaled to the unit square.

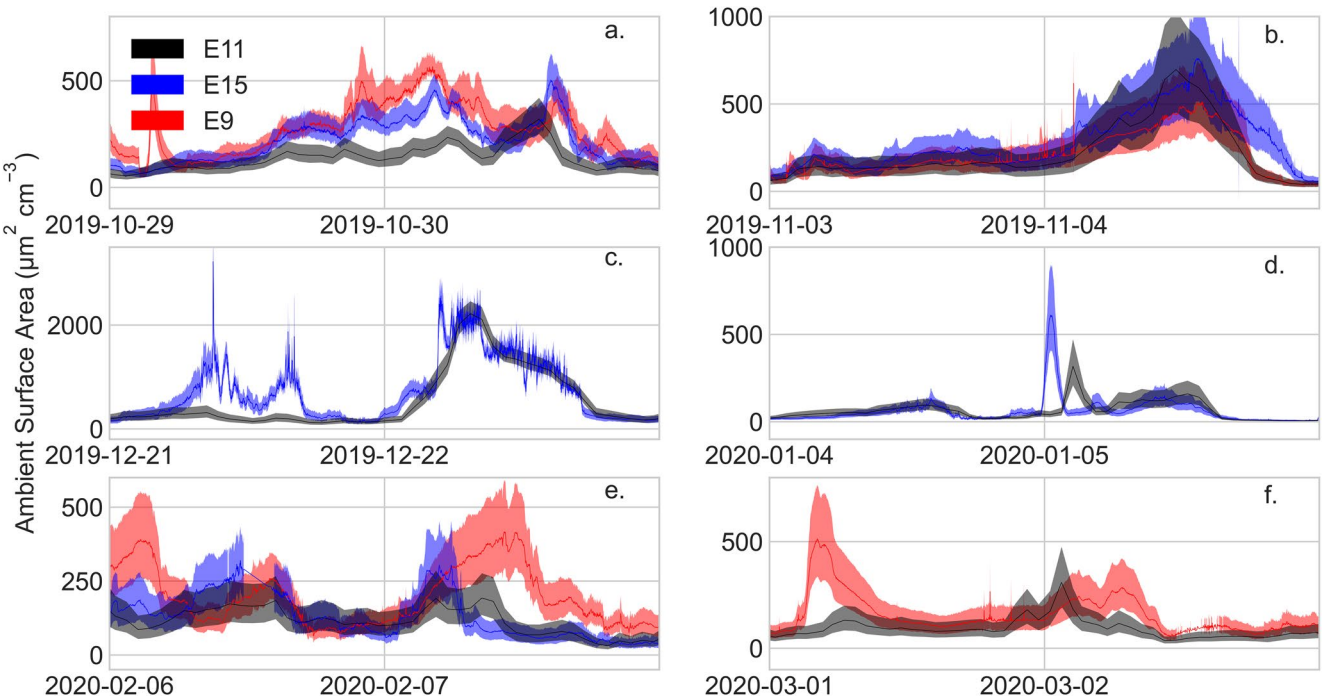

Figure 7. A_140 from stations with duplicate pairs measuring during 3-day periods each month. The shaded region shows the total uncertainty in surface area, which is defined as a combination of the theoretical uncertainty in sizing accuracy (systematic error) and measurement error (Equation S3 in Supporting Information S1).

4. Conclusions

POPSnet-SGP demonstrates a new approach to quantify measurement representation error for future model evaluation using a spatially dense network of robust research-grade instruments. Our data suggest N_140 measurement representation error remains ≤30% for a 1-day averaging period. Representation error in N_140, A_140, and N_400 decreased with increasing averaging periods (1 min–1 day) by 30%–45% and routinely exceeded the POPS measurement error (e.g., 4.5% ± 3.2%; mean ± 1σ for N_140). To the best of our knowledge, this study is the first to estimate the total uncertainty in A_140, comprised of measurement error and the potential error from an assumed index of refraction needed to size aerosols using an aerosol spectrometer. Differences in the mean representation error between stations (e.g., >10% for both N_140 and A_140 given a 30-min averaging period) illustrate the importance of site selection and suggest that the central facility is well suited for large-scale regional studies. Our measurements provide insight into the transport across the SGP region, occasional localized primary aerosol emissions, and the influence of local meteorology leading to measurement representation error. Continued monitoring of representation error at ARM-SGP and studies in other regions are needed to confirm these findings.

We anticipate that POPSnet-SGP measurements will be useful for global aerosol models. With few large local aerosol sources (e.g., cities) nearby (Parworth et al., 2015), it is expected that aerosol across the ARM-SGP region is largely representative of background continental air masses (McComiskey et al., 2008; McComiskey and Ferrare, 2016). As a result, information on the representation error in the Southern Great Plains region may establish a prior for the representation error of other remote regions and could be scalable over similar large areas of the globe. Comparisons between tower-based and ground-based POPS are needed to determine if a near surface in situ aerosol measurement is representative of the BL during the day, and confirm to what extent these become decoupled at night. We expect that the expansion of POPSnet to other, more heterogenous environments would reveal greater spatial variability in aerosol distributions with an increased likelihood of measurement representation errors >100%.

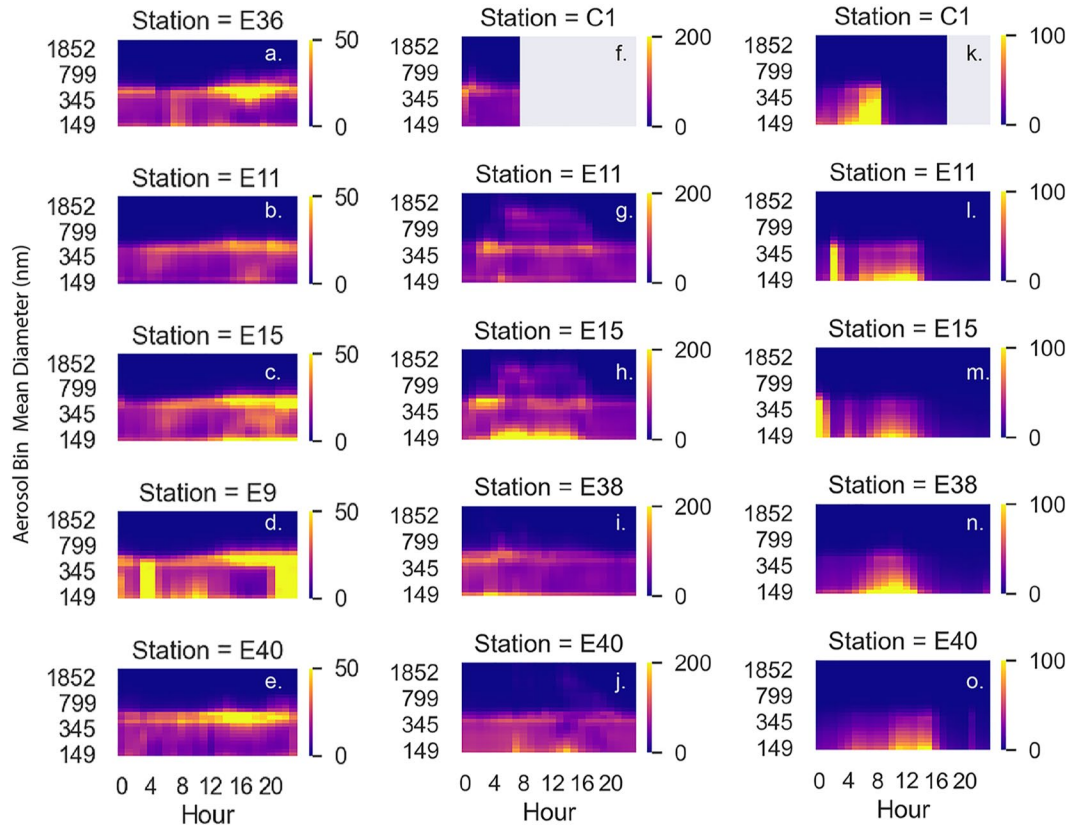

Figure 8. Number concentration versus time from five operational sites over 24-hr periods when stations with pairs of Portable Optical Particle Spectrometer (POPS) indicated significantly different A_140 time series on three dates, 29 October 2019 (a)–(e), 22 December (f)–(j), and 5 January (k)–(o). Note different color scaling and color bars for each date.

Data Availability Statement

The data for this publication may be found at https://csl.noaa.gov/projects/popsnet/dataview.html, and are publicly available. The ancillary meteorological data (i.e., 1-min mean of atmospheric temperature, relative humidity, corrected total precipitation, and wind velocity) may be found at https://adc.arm.gov/discovery/#/results/s::sgp-met, and the AERONET level 2.0 data may be downloaded for the ARM-SGP site at https://aeronet.gsfc.nasa.gov/cgi-bin/webtool_aod_v3.

Acknowledgments
We would like to thank the staff at ARM-SGP for their help in the deployment and support of POPSnet-SGP. Meteorological data were obtained from the ARM-SGP facility, a U.S. Department of Energy Office of Science User Facility managed by the Biological and Environmental Research Program.

References

Aldhaif, A. M., Stahl, C., Braun, R. A., Moghaddam, M. A., Shingler, T., Crosbie, E., et al. (2018). Characterization of the real part of dry aerosol refractive index over North America from the surface to 12 km. *Journal of Geophysical Research: Atmospheres*, *123*(15), 8283–8300. https://doi.org/10.1029/2018JD028504

Andrews, E., Sheridan, P. J., Fiebig, M., McComiskey, A., Ogren, J. A., Arnott, P., et al. (2006). Comparison of methods for deriving aerosol asymmetry parameter. *Journal of Geophysical Research*, *111*, D05S04. https://doi.org/10.1029/2004JD005734

Bellouin, N., Quaas, J., Gryspeerdt, E., Kinne, S., Stier, P., Watson-Parris, D., et al. (2020). Bounding global aerosol radiative forcing of climate change. *Reviews of Geophysics*, *58*, e2019RG000660. https://doi.org/10.1029/2019RG000660

Bond, T. C., Doherty, S. J., Fahey, D. W., Forster, P. M., Berntsen, T., DeAngelo, B. J., et al. (2013). Bounding the role of black carbon in the climate system: A scientific assessment. *Journal of Geophysical Research: Atmospheres*, *118*, 5380–5552. https://doi.org/10.1002/jgrd.50171

Bulot, F. M. J., Johnston, S. J., Basford, P. J., Easton, N. H. C., Cox, S. J., Foster, G. L., et al. (2019). *Long-term field comparison of multiple low-cost particulate matter sensors in an outdoor urban environment*. https://doi.org/10.5281/ZENODO.2605402

Carslaw, K. S., Lee, L. A., Reddington, C. L., Pringle, K. J., Rap, A., Forster, P. M., et al. (2013). Large contribution of natural aerosols to uncertainty in indirect forcing. *Nature*, *503*(7474), 67–71. https://doi.org/10.1038/nature12674

Cassanelli, P., Johnson, D., & Anthony Cox, R. (2005). A temperature-dependent relative-rate study of the OH initiated oxidation of n-butane: The kinetics of the reactions of the 1- and 2-butoxy radicals. *Physical Chemistry Chemical Physics*, *7*(21), 3702. https://doi.org/10.1039/b507137b

Chang, K.-L., Cooper, O. R., Gaudel, A., Petropavlovskikh, I., & Thouret, V. (2020). Statistical regularization for trend detection: An integrated approach for detecting long-term trends from sparse tropospheric ozone profiles. *Atmospheric Chemistry and Physics*, *20*(16), 9915–9938. https://doi.org/10.5194/acp-20-9915-2020

Chang, K.-L., Petropavlovskikh, I., Copper, O. R., Schultz, M. G., & Wang, T. (2017). Regional trend analysis of surface ozone observations from monitoring networks in eastern North America, Europe and East Asia. *Elementa: Science of the Anthropocene*, *5*, 50. https://doi.org/10.1525/elementa.243

Ferrare, R. A., Melfi, S. H., Whiteman, D. N., Evans, K. D., Poellot, M., & Kaufman, Y. J. (1998). Raman lidar measurements of aerosol extinction and backscattering: 2. Derivation of aerosol real refractive index, single-scattering albedo, and humidification factor using Raman lidar and aircraft size distribution measurements. *Journal of Geophysical Research*, *103*(D16), 19673–19689. https://doi.org/10.1029/98JD01647

Gao, R. S., Telg, H., McLaughlin, R. J., Ciciora, S. J., Watts, L. A., Richardson, M. S., et al. (2016). A light-weight, high-sensitivity particle spectrometer for PM2.5 aerosol measurements. *Aerosol Science and Technology*, *50*(1), 88–99. https://doi.org/10.1080/02786826.2015.1131809

Haywood, J., & Boucher, O. (2000). Estimates of the direct and indirect radiative forcing due to tropospheric aerosols: A review. *Reviews of Geophysics*, *38*(4), 513–543. https://doi.org/10.1029/1999RG000078

Janjić, T., Bormann, N., Bocquet, M., Carton, J. A., Cohn, S. E., Dance, S. L., et al. (2018). On the representation error in data assimilation. *Quarterly Journal of the Royal Meteorological Society*, *144*(713), 1257–1278. https://doi.org/10.1002/qj.3130

Johnson, J. S., Regayre, L. A., Yoshioka, M., Pringle, K. J., Turnock, S. T., Browse, J., et al. (2020). Robust observational constraint of uncertain aerosol processes and emissions in a climate model and the effect on aerosol radiative forcing. *Atmospheric Chemistry and Physics*, *20*(15), 9491–9524. https://doi.org/10.5194/acp-20-9491-2020

Li, Z. (2002). Impact of surface inhomogeneity on solar radiative transfer under overcast conditions. *Journal of Geophysical Research*, *107*(D16), 4294. https://doi.org/10.1029/2001JD000976

Lohmann, U., & Feichter, J. (2005). Global indirect aerosol effects: A review. *Atmospheric Chemistry and Physics*, *5*(3), 715–737. https://doi.org/10.3929/ETHZ-B-000033632

Lorenc, A. C. (1986). Analysis methods for numerical weather prediction. *Quarterly Journal of the Royal Meteorological Society*, *112*(474), 1177–1194. https://doi.org/10.1002/qj.49711247414

Mann, G. W., Carslaw, K. S., Reddington, C. L., Pringle, K. J., Schulz, M., Asmi, A., et al. (2014). Intercomparison and evaluation of global aerosol microphysical properties among AeroCom models of a range of complexity. *Atmospheric Chemistry and Physics*, *14*(9), 4679–4713. https://doi.org/10.5194/acp-14-4679-2014

McComiskey, A., & Ferrare, R. A. (2016). Aerosol physical and optical properties and processes in the ARM program. *Meteorological Monographs*, *57*(1), 21.1–21.17. https://doi.org/10.1175/AMSMONOGRAPHS-D-15-0028.1

McComiskey, A., Schwartz, S. E., Schmid, B., Guan, H., Lewis, E. R., Ricchiazzi, P., & Ogren, J. A. (2008). Direct aerosol forcing: Calculation from observables and sensitivities to inputs. *Journal of Geophysical Research*, *113*, D09202. https://doi.org/10.1029/2007JD009170

Michalsky, J. (2003). Simultaneous spectral albedo measurements near the Atmospheric Radiation Measurement Southern Great Plains (ARM SGP) central facility. *Journal of Geophysical Research*, *108*(D8), 4254. https://doi.org/10.1029/2002JD002906

Murphy, D. M., Froyd, K. D., Bourgeois, I., Brock, C. A., Kupc, A., Peischl, J., et al. (2021). Radiative and chemical implications of the size and composition of aerosol particles in the existing or modified global stratosphere. *Atmospheric Chemistry and Physics*. https://doi.org/10.5194/acp-21-8915-2021

Myhre, G., Kvalevåg, M., Rädel, G., Cook, J., Shine, K. P., Clark, H., et al. (2009). Intercomparison of radiative forcing calculations of stratospheric water vapour and contrails. *Meteorologische Zeitschrift*, *18*(6), 585–596. https://doi.org/10.1127/0941-2948/2009/0411

Noble, S. R. & Hudson, J. G. (2019). Effects of continental clouds on surface Aitken and accumulation modes. *Journal of Geophysical Research: Atmospheres*, *124*(10), 5479–5502. https://doi.org/10.1029/2019JD030297

Parworth, C., Fast, J., Mei, F., Shippert, T., Sivaraman, C., Tilp, A., et al. (2015). Long-term measurements of submicrometer aerosol chemistry at the Southern Great Plains (SGP) using an Aerosol Chemical Speciation Monitor (ACSM). *Atmospheric Environment*, *106*, 43–55. https://doi.org/10.1016/j.atmosenv.2015.01.060

Piedrahita, R., Xiang, Y., Masson, N., Ortega, J., Collier, A., Jiang, Y., et al. (2014). The next generation of low-cost personal air quality sensors for quantitative exposure monitoring. *Atmospheric Measurement Techniques*, *7*(10), 3325–3336. https://doi.org/10.5194/amt-7-3325-2014

Reddington, C. L., Carslaw, K. S., Stier, P., Schutgens, N., Coe, H., Liu, D., et al. (2017). The Global Aerosol Synthesis and Science Project (GASSP): Measurements and modeling to reduce uncertainty. *Bulletin of the American Meteorological Society*, *98*(9), 1857–1877. https://doi.org/10.1175/BAMS-D-15-00317.1

Schutgens, N., Tsyro, S., Gryspeerdt, E., Goto, D., Weigum, N., Schulz, M., & Stier, P. (2017). On the spatio-temporal representativeness of observations. *Atmospheric Chemistry and Physics*, *17*(16), 9761–9780. https://doi.org/10.5194/acp-17-9761-2017

Schwarz, J. P., Gao, R. S., Spackman, J. R., Watts, L. A., Thomson, D. S., Fahey, D. W., et al. (2008). Measurement of the mixing state, mass, and optical size of individual black carbon particles in urban and biomass burning emissions. *Geophysical Research Letters*, *35*, L13810. https://doi.org/10.1029/2008GL033968

Sisterson, D. L., Peppler, R. A., Cress, T. S., Lamb, P. J., & Turner, D. D. (2016). The ARM Southern Great Plains (SGP) Site. *Meteorological Monographs*, *57*(1), 6.1–6.14. https://doi.org/10.1175/AMSMONOGRAPHS-D-16-0004.1

Wood, S. (2017). *Generalized additive models: An introduction with R* (2nd ed., 496 pp.). CRC Press.